Monte Carlo Simulations and Spectroscopic Studies of the Sorption and Cosorption of Group VI Metal Hexacarbonyls in Faujasitic Zeolites

Claude Brémard,* Gabrielle Ginestet, Jacky Laureyns, and Marielle Le Maire

Contribution from the Laboratoire de Spectrochimie infrarouge et Raman, UPR-CNRS 2631, Bât. C5, Université des Sciences et Technologies de Lille, 59655 Villeneuve d'Ascq cedex, France

Received December 28, 1994[⊗]

Abstract: Molecular simulations of the sorption and cosorption energetics and siting locations of $M(CO)_6$ (M = Cr, Mo, W) in faujasitic M'_nFAU zeolites (n = 0−96, Si/Al = 100−1, extraframework cations M' = Li^+, Na^+, K^+, Rb^+, Cs^+, Mg^{2+}, and Ca^{2+}) have been presented in combination with Diffuse Reflectance Infrared Fourier Transform Spectroscopy (DRIFTS), Attenuated Total Reflectance (ATR-FTIR), and Raman scattering experimental study at low temperature. From the present Monte Carlo calculations and the earlier and present experimental works a coherent picture of the sorption and the cosorption of $M(CO)_6$ has been drawn as a function of the Si/Al ratio of the zeolite framework, the cation size, and the cationic site occupancy as well as the coverage of the sorbates. The most favorable siting regions of the completely siliceous FAU zeolite pore space are the windows of the supercages, with intercage and intracage rapid motions of the $M(CO)_6$ molecules. In aluminated M'_nFAU zeolites the calculated average energy provides evidence to the contribution of significant site II cation/sorbate interactions whereas the site I,I' cation/sorbate and sorbate/sorbate interactions remain weak even at high loading. In $M'_{56}FAU$ zeolites with bulky cations (M' = K^+, Rb^+, Cs^+), the $M(CO)_6$ molecules are rigidily held within the windows of the supercages to the six octahedral disposed site II cations. The sorption sites are randomly filled from low coverage to saturation. In $M'_{56}FAU$ zeolites with small cations (M' = Li^+, Na^+), the distribution of positions occupied by $M(CO)_6$ is located in the vicinity of the windows. It is suggested that $M(CO)_6$ is predominently entrapped as an isolated molecule at low coverage whereas at high loading the filling is primarily pairwise. In $M'_{28}FAU$ zeolites with site II partial occupancy (M' = Mg^{2+}, Ca^{2+}), the distribution of positions occupied by $M(CO)_6$ is located in the vicinity of the windows in two slightly different sorption sites.

Introduction

There has been considerable interest in recent years in the species formed on the sorption of metal carbonyls on oxide surfaces, such as silica, alumina, and porous aluminosilicate materials such as zeolites.[1,2] Intrazeolite topotaxy can be envisioned to provide an attractive mean whereby organometallic precursor molecules can be encapsulated and precisely organized in the void space.[3−6] Despite the large volume of work associated with metal carbonyl complexes encapsulated in zeolites, there has been very little work aimed at the siting location and intermolecular interactions between metal carbonyl complexes such as hexacarbonyls(0) within the cavity network of zeolites.[7−24] Hence, it is of interest to investigate the location and the motions of these molecules inside the cavities of molecular sieves and compare the behavior to that obtained in solution or in the crystal lattice.

The electrodynamic interactions between molecules in close proximity can induce frequency shifts, band splittings, and intensity transfers in infrared and Raman spectra. These changes are likely to be of greatest importance in vibrational spectra from cristalline solids, from structurally heterogeneous substrates such as supported catalysts, as well as from guests in the void volume of porous materials. To date, however, few well-resolved IR spectra of zeolite-sorbed hexacarbonyls(0) have been reported and those that have do not agree in detail with the

[⊗] Abstract published in *Advance ACS Abstracts*, August 15, 1995.

(1) Bailey, D. C.; Langer, S. H. *Chem. Rev.* **1981**, *81*, 109.
(2) Jacobs, P. A.; Jaeger, N. I.; Jiru, P.; Schulz-Ekloff, G., Eds. *Metal Microstructures in Zeolites*; Elsevier: Amsterdam, 1982.
(3) Ozin, G. A.; Gil, C. *Chem. Rev.* **1989**, *89*, 1749 and references cited therein.
(4) Ozin, G. A.; Kuperman, A.; Stein, A. *Adv. Mater.* **1989**, *101*, 373.
(5) Stucky, G. D.; Mac Dougall, J. *Science* **1990**, *247*, 669 and references cited therein.
(6) Ozin, G. A.; Steele, M. R.; Holmes, A. J. *Chem. Mater.* **1994**, *6*, 999.
(7) Coudurier, G.; Gallezot, H.; Praliaud, H.; Primet, M.; Imelik, B. *C. R. Acad. Sci. Paris C* **1976**, *282*, 311.
(8) Bein, T.; Jacobs, P. A. *J. Chem. Soc., Faraday Trans.* **1983**, *79*, 1919.
(9) You-sing, Y.; Howe, R. F. *J. Chem. Soc., Faraday Trans. 1* **1986**, *82*, 2887.
(10) Özkar, S.; Ozin, G. A.; Moller K.; Bein, T. *J. Am. Chem. Soc.* **1990**, *112*, 9575 and references cited therein.
(11) Li, X.; Ozin, G. A.; Özkar, S. *J. Phys. Chem.* **1991**, *95*, 4463.
(12) Borvornwattananont, A.; Moller, K.; Bein, T. *J. Phys. Chem.* **1989**, *93*, 4205.
(13) Ozin, G. A.; Özkar, S.; Macdonald, P. *J. Phys. Chem.* **1990**, *94*, 6939.
(14) Ozin, G. A.; Haddleton, D. M.; Gil, C. J. *J. Phys. Chem.* **1989**, *93*, 6710.
(15) Ozin, G. A.; Özkar, S. *Chem. Mater.* **1992**, *4*, 511.
(16) Moller, K.; Bein, T.; Özkar, S.; Ozin, G. A. *J. Phys. Chem.* **1991**, *95*, 5276.
(17) Connaway, M. C.; Hanson, B. E. *Inorg. Chem.* **1986**, 25, 1445.
(18) Bein, T.; Mc Lain, S. J.; Corbin, D. R.; Farlee, R. D.; Moller, K.; Stucky, G. D.; Woolery, G.; Sayers, D. *J. Am. Chem. Soc.* **1988**, *110*, 1801.
(19) Pastore, O. H.; Ozin, G. A.; Poë, A. J. *J. Am. Chem. Soc.* **1993**, *115*, 1215.
(20) Cybulski, P. A.; Gillis, D. J.; Baird, M. C. *Inorg. Chem.* **1993**, *32*, 460.
(21) Brémard, C.; Denneulin, E.; Depecker, C.; Legrand, P. *Struct. React. Surf.* **1989**, 228.
(22) Brémard, C.; Des Grousilliers, H.; Depecker, C.; Legrand, P. *Proceedings of the International Workshop on Fourier Transform Infrared Spectroscopy*; Vansant, E. F., Ed.; Antwerp, Belgium; 1990, p 84.
(23) Brémard, C.; Des Grousilliers, H.; Depecker, C.; Legrand, P. *J. Chem. Soc., Chem. Commun.* **1991**, 1411.
(24) Brémard, C.; Des Grousilliers, H.; Depecker, C.; Legrand, P. *Appl. Spectrosc.* **1991**, *45*, 1278.

0002-7863/95/1517-9274$09.00/0

proposed siting location.[20] Some new perspectives in this field come from the Diffused Reflectance Infrared Fourier Transform Spectroscopy (DRIFTS),[21-24] Attenuated Total Reflectance (ATR-FTIR), and Raman spectroscopy[25,26] as well as from predictions of energetics and siting locations of sorbates from Grand Canonical Monte Carlo simulations. Monte Carlo simulations of hydrocarbons in zeolites at infinite dilution have been used by several authors to calculate sites of minimum energy within the zeolite lattice and heats of sorption.[27] However, the important problem of predicting the sorption at higher loading scarcely has been addressed to date.[28]

The $M(CO)_6$ molecules (M = Cr, Mo, W) have diameters in the range 7.4−7.6 Å and can therefore gain free access to the 13-Å diameter α-cage through the 8.0-Å diameter 12-ring entrance port of faujasitic zeolites. The faujasitic zeolites, abbreviated hereafter as M'_nFAU, are cristalline aluminosilicates with silicon/aluminum ratios (Si/Al) of the framework in the 1−100 range. M′ is the counter balancing extraframework cation (M′ = Li^+, Na^+, K^+, Rb^+, Cs^+, Mg^{2+}, and Ca^{2+}). The void space of the α-cage M'_nFAU material is reduced by bulky cations such as M′ = Cs^+, which protrude deeper into the body of the α-cage than their lighter congeners, such as M′ = Li^+. An important, recurring question that arises in the study of occluded sorbates is one regarding the number, the location, and the distribution of the guest molecules trapped in the voids of the host.

Our main objective here is to explore how siting location and distribution in the void space vary with the loading, the Si/Al ratio of the framework, and the size of the extraframework cation M′. In the present work, we report the room and low-temperature Raman, DRIFTS, and ATR-FTIR spectroscopic studies of hexacarbonyls(0), $M(CO)_6$ (M = Cr, Mo, W), sorbed and cosorbed in faujasitic FAU zeolites. The spectral diagnostics of the guest and/or host are monitored over a large range of Si/Al ratio, over a large range of loading, and over a specified temperature range. They are supported by Grand Canonical Monte Carlo simulations of the sorptions. The spectroscopic and modeling results reveal informative clues about guest location and spatial distribution of hexacarbonyl(0) molecules trapped in the voids of the porous materials.

Experimental Section

Materials. The completely siliceous FAU zeolite (Si/Al > 100) obtained by hydrothermal treatment was kindly provided by Degussa. The unit cell composition is $Si_{192}O_{384}{\cdot}nH_2O$. The partialy dealuminated samples were kindly provided by G. Descat and S. Tretjak (Grande Paroisse SA). After exhaustive exchange by Na^+, the unit cell compositions were found to be $Na_4Al_4Si_{188}O_{384}{\cdot}nH_2O$ (Si/Al = 44), $Na_6Al_6Si_{186}O_{384}{\cdot}nH_2O$ (Si/Al = 32), and $Na_9Al_9Si_{188}O_{384}{\cdot}nH_2O$ (Si/Al = 20), respectively. The $Na_{41}FAU$ sample (Si/Al = 3.8) was kindly provided by J. M. Manoli and C. Potvin (Laboratoire de Réactivité de Surface, Université P. and M. Curie, Paris). The $Na_{56}FAU$ zeolite (Si/Al = 2.49) was obtained from Union Carbide. The exchanged zeolites $Li_{50}Na_6FAU$, $K_{51}Na_5FAU$, $Rb_{52}Na_4FAU$, $Cs_{48}Na_8FAU$, $Mg_{25}Na_6FAU$, and $Ca_{25}Na_6FAU$ were obtained as previously described.[29] The unit cell compositions of the exchanged zeolites were found to be in good agreement with the above formula. The $Na_{85}FAU$ (Si/Al = 1.26) and $Na_{96}FAU$ (Si/Al = 1) samples were kindly provided by X. Reymonet (CECA). The average crystallite size of all the zeolite samples was 0.5 μm and the average particle size was 5 μm.

$M(CO)_6$ (where M = Cr, Mo, W) were purchased from Strem Chemicals Inc. and used after dehydration.

Techniques. The FTIR spectrometer was a Bruker IFS 113v instrument equipped with a liquid nitrogen cooled MCT detector (mid-IR) and a He-cooled bolometer detector (far-IR) with the convenient beam splitters. The OPUS Bruker software was used for spectral acquisition, storage, manipulation, and plotting. The spectra were recorded at 2-cm^{-1} resolution.

The main previous vibrational results[7-20] of intrazeolite group VI metal hexacarbonyls are based on IR spectroscopic studies at room temperature in the stretching ν(CO) region. The technique used was the transmission technique through a thin self-supporting wafer of zeolite (0.1 mm). The ATR-FTIR and Raman spectroscopies are not sensitive enough to provide spectral diagnostics of the sorption of $M(CO)_6$ at low coverage. In contrast, the DRIFTS reveals informative ν(CO) patterns at very low coverage in a wide range of temperature, 100−330 K. The volume of powder viewed by the DRIFTS technique corresponds approximately to a disc 4 mm in diameter and 1 mm in depth. This particularity is very efficient for studying the sorption at very low coverage, typically less than 1 $M(CO)_6$ per 20 unit cells.[22] The key part of the "in situ" DRIFTS apparatus is a modified version of a Harrick Scientific Diffuse Reflectance Attachement "DRA-2CI" Praying mantis and "HVC-DRP" cell equipped with CaF_2 windows, operating from 100 to 800 K. Conventionally, an equation derived from the Kubelka−Munk phenomenogical theory[30] is used in order to relate a chromophore concentration to the intensity of the sample diffuse reflection. In this equation, $F(R) = (1 - R)^2/2R = K/S$, the sample is treated as a continuum, R represents the ratio of the diffuse reflectance of the loaded zeolite to that of the dehydrated neat zeolite, K designates an absorption coefficient proportional to the concentration C of the chromophore, and S is the scattering coefficient of the powder. The penetration depth in the powder was estimated to be 1 mm.[31] The far-IR spectra were recorded using the transmission technique through a self-supporting wafer contained in a heatable evacuable cell equipped with silicon windows.

The ATR (Attenuated Total Reflectance) FT-IR spectra were recorded at room temperature using a horizontal ZnSe crystal accessory (Specac model, 45°, 6 reflections). The penetration depth in the powder was estimated to be approximately 0.5 μm around 2000 cm^{-1}.[32]

The Raman spectra were recorded at room and low temperature using a multichannel X−Y Dilor spectrometer, in the 2200−1900 cm^{-1} spectral range at 3-cm^{-1} resolution, whereas a Dilor RTI triple monochromator is more suitable to record the low-frequency Raman spectra at 5-cm^{-1} resolution. Dilor and Spectracalc software were used for spectral acquisition, storage, manipulation, and plotting. The exciting radiations used were 514.5 and 565.2 nm from a Spectra-physics Ar^+ and Kr^+ laser, respectively. To avoid thermal or photochemical decomposition of entrapped carbonyl metals the spectra were recorded using the sample spinning technique at room temperature or using a cylindrical lens and a static sample at 77 K with less than 50 mW at the sample.

The cristallinity and the purity of the dehydrated and loaded samples were checked by X-ray powder diffraction patterns (XRD). The elemental analyses for Na, Al, Cr, and Mo were obtained using the ICP technique.

The modeling results published herewith were generated using the program Cerius 3.2 developped by Molecular Simulations Inc.

Sorption of $M(CO)_6$ in Zeolites. Up stream of the DRIFTS cell are vacuum and gas lines (He, CO, O_2) and a reaction delivery system.[22] The solid $M(CO)_6$ was stocked in a by-pass system and $M(CO)_6$ vapor was admitted into the cell by sweeping solid $M(CO)_6$ into the dry He carrier stream. The rate of delivery was controlled by adjusting the temperature of the solid and the He flow rate. The sequence of steps in a typical adsorption experiment was as follows: the powdered zeolite sample is introduced into the cell connected to the vacuum line. The sample is pumped down to a pressure of 10^{-3} Pa and heated stepwise to 700 K, then O_2 gas is admitted into the cell. After 6 h, the sample is pumped down to a pressure of 10^{-3} Pa and then cooled to room

(25) Brémard, C.; Des Grousilliers, H. *J. Raman Spectrosc.* **1991**, *22*, 125.
(26) Brémard, C.; Bougeard, D. *Adv. Mater.* **1995**, *7*, 10.
(27) Smit, B.; den Outen, C. J. J. *J. Phys. Chem.* **1988**, *92*, 7169.
(28) Snurr, R. Q.; Bell, A. T.; Theodorou, D. N. *J. Phys. Chem.* **1993**, *97*, 13752 and references cited therein.
(29) Brémard, C.; Le Maire, M. *J. Phys. Chem.* **1993**, *97*, 9695.
(30) Kubelka, P.; Munck, F. *Z. Tech. Phys.* **1931**, *12*, 593.
(31) Fraser, D. J. J.; Griffiths, P. R. *Appl. Spectrosc.* **1990**, *44*, 193.
(32) Smith-Palmer, T.; Lynch, B. M.; Roberts, C.; Lü, Y. *Appl. Spectrosc.* **1991**, *45*, 1022.

temperature. He carrier gas is drawn through the dry zeolite. A reference spectrum of the neat zeolite is run subsequently. The side arm containing the solid $M(CO)_6$ is opened for different periods and spectra are recorded after each period during and after the equilibrium phase at different temperatures in the 100−330 K range. At low coverage, the equilibrium period of loaded FAU zeolites (Si/Al > 2.5) was estimated to be 24 h under He in the DRIFTS cell; this period can be reduced to 6 h under gentle warming. Unfortunately, it should be noted that the decomposition of $M(CO)_6$ occurs in FAU zeolites (Si/Al < 2.5) some hours after the loading at room temperature. So, the significant DRIFTS spectra of loaded FAU zeolites (Si/Al < 2.5) were recorded after an equilibrium period of 12 h at 0 °C. At low coverage the loading of $M(CO)_6$ was obtained through the infrared intensity using the Kubelka−Munk scale $f(R) = (1 - R^2)/2R$ which is assumed to be proportional to the $M(CO)_6$ concentration. The calibration was obtained by taking as standard the ν(CO) intensity of three higher loaded zeolites. Quantification of the degree of incorporation of the organometallic into these zeolites was determined by elementary analysis (see above). Some IR microspectrometric measurements have been carried out; they reveal homogeneous loading in the limit of the spacial resolution (80 μm^3) of the technique.

A previously described procedure was used for *in situ* transmission of far-IR spectroscopic studies taking self-supporting zeolite wafers as samples.[10]

To perform higher coverages the loadings were undertaken in a vertical quartz reactor where the powdered zeolites were exposed after dehydration to the full vapor pressure of $M(CO)_6$ (M = Cr, Mo, W) under flowing helium over 48 h at room temperature followed by evacuation for 30 min and stocked under dry argon. After 2 weeks the sample was transferred under dry argon, either in the DRIFTS cell or in the ATR cell or in the XRD cell or in cylindrical glass tubes for Raman experiments and elemental analyses. These experimental procedures were assumed to give fully equilibrated samples. We notice that all the chemical and physical properties of the samples remained identical over several years when the loaded zeolites (Si/Al > 2.5) were stocked in sealed tubes and in the dark. The DRIFTS spectra were recorded using the raw compound as a sample or after dispersion in dehydrated NaA zeolite as solid diluent to avoid the saturation of the fundamentals.

Theoretical Methods. The atomic positions for the zeolite hosts were obtained from all the available X-ray or neutron diffraction determinations of the structures.[33−39] In the simulations the silicon, aluminum, and oxygen atoms of the zeolite framework and extraframework cations are assumed to be fixed at the crystallographic coordinates determined from structural data. The substitutional Si, Al disorder was applied according to the Lowenstein rule. The partial occupancy of extraframework cation sites was taken into account explicitely in view of the extensive structural work published in the literature.[34−39] From X-ray powder diffraction studies Van Dun *et al.* concluded that the influence of adsorbed molecules on the cation distribution increases with the cation−molecule interaction energy.[40] In the case of the adsorption of hydrophobic molecules such as benzene the extraframework cation distribution was found negligible. Fitch *et al.* reported a shift of 0.009 nm of Na^+ cations in Na_{56}FAU due to the interaction of benzene.[35] The interaction of intrazeolite $Mo(CO)_6$ with rubidium cations of the zeolite has been probed previously with rubidium edge EXAFS data.[10] The data of the empty rubidium exchanged zeolite as well as the $Mo(CO)_6$ loaded sample were found to be very similar.

Table 1. Summary of the Potential Parameters Used To Represent the Zeolite−Sorbate Interactions

zeolite or sorbate atom	sorbate atom	A_{ij} (kcal mol^{-1} Å^{12})	B_{ij} (kcal mol^{-1} Å^6)
zeolite			
Si	O	154 669.7	111.2
Si	C	108 788.8	72.3
Al	O	154 669.7	111.2
Al	C	108 788.8	72.3
O	O	23 058.4	42.9
O	C	33 357.8	51.6
Li^+	O	363.7	4.2
Li^+	C	920.4	12.4
Na^+	O	23 447.1	106.1
Na^+	C	5 037.3	29.1
K^+	O	42 457.8	142.8
K^+	C	33 081.8	74.6
Rb^+	O	77 764.1	193.2
Rb^+	C	48 422.7	90.2
Cs^+	O	266 797.4	357.8
Cs^+	C	96 748.8	127.5
Ca^{2+}	O	23 447.1	106.1
Ca^{2+}	C	5 037.3	29.1
sorbate	sorbate atom		
O	O	131 659.0	102.6
C	C	197 488.6	153.9
C	O	162 568.0	120.5

The error made by fixing the cation positions throughout the calculations of $M(CO)_6$ in M'_nFAU therefore is assumed negligible. $M(CO)_6$ is modeled as rigid octahedral molecules. The M−C and C−O bond lengths are obtained from electronic diffraction data (M = Cr, Mo)[41] or from X-ray diffraction studies (M = Cr, Mo, W).[42,43] In addition the weak deformations of the $M(CO)_6$ skeleton which occur upon sorption are assumed to be negligible according to previous EXAFS results.[10,16]

The zeolite (Z) and the sorbates (S) are assumed to interact through pairwise-additive potential between atoms of the guests and atoms of the host (U_{ZS}). For simulations at higher loadings, the interactions between sorbates (U_{SS}) must also be included. The atom−atom interactions are modeled with a Lennard-Jones plus point-charge potential,

$$U_{ZS} = \sum_{ij} A_{ij}/r_{ij}^{12} - B_{ij}/r_{ij}^{6} + \sum_{ij} qiqj/rij \qquad (1)$$

$$U_{SS} = \sum_{ik} A_{jk}/r_{jk}^{12} - B_{jk}/r_{jk}^{6} + \sum_{jk} qjqk/rjk \qquad (2)$$

where i and j,k are atoms of the M'_nFAU (Z) host and $M(CO)_6$ (S) guests, respectively, and r_{ij} and r_{jk} are the distance between them. A and B are the Lennard-Jones constants and q is the partial charge of the atoms. The Lennard-Jones potential accounts for dispersive and repulsive interactions and the values used throughout the present work were taken from the literature[27,28,44−48] and are listed in Table 1 as A_{ij} and B_{ij} parameters. The charge distribution within FAU-type structures was taken from ref 39. FAU: Si, (+1.59); O, (−0.77 to −0.79). M'_{56}-FAU: Si, (+1.42 to +1.45); Al, (+1.23); O, (−0.75 to −0.89); M′, (+1). M'_{96}FAU: Si, (+1.26); Al, (+1.13); O, (−0.82 to −0.88); M′, (+1). Theoretical studies of the metal−ligand coordinate bond in the metal carbonyls, especially $Cr(CO)_6$, are numerous.[49] They suggest that the concept of localized partial charge can be used efficiently. The

(33) Hriljac, J. A.; Eddy, M. M.; Cheetham, A. K.; Donohue, J. A.; Ray, G. J. *J. Solid State Chem.* **1993**, *106*, 66.
(34) Lievens, J. L.; Mortier, W. J.; Chao, K. J. *J. Phys. Chem. Solids* **1992**, *53*, 1163.
(35) Fitch, A. N.; Jobic, H.; Renouprez, A. *J. Phys. Chem.* **1986**, *90*, 1311.
(36) Mortier, W. J. Compilation of Extra-framework Sites in Zeolites; issued by the commission of the international zeolite Association, 1981.
(37) Forano, C.; Slade, C. T. R.; Krog Andersen, E.; Krog Andersen, I. G.; Prince F. *J. Solid State Chem.* **1989**, *82*, 95.
(38) Bennett, J. M.; Smith, J. B. *Mater. Res. Bull.* **1968**, *92*, 633.
(39) Uytterhoeven, L.; Dompas, D.; Mortier, W. J. *J. Chem. Soc., Faraday Trans*, **1992**, *3*, 633 and references cited therein.
(40) Van Dun, J. J. L.; Mortier, W. J.; Uytterhoeven, J. B. *Zeolites* **1985**, *5*, 257.
(41) Arnesen, S. P.; Seip, H. M. *Acta Chim. Scand.* **1966**, *20*, 2711.
(42) Jost, A.; Rees, B. *Acta Crystallogr.* **1975**, *B31*, 2647.
(43) Whitaker, A.; Jeffery, J. W. *Acta Crytallogr.* **1967**, *23*, 977.
(44) Brubeker, G. R.; Johnson, D. W. *Coord. Chem. Rev.* **1984**, *53*, 1.
(45) Kiselev, A. V.; Lopatikin, A. A.; Shulga, A. A. *Zeolites* **1985**, *5*, 261.
(46) Besus, A. G.; Kocirik, M.; Kiselev, A. V.; Lopatkin, A. A.; Vasilyeva, E. A. *Zeolites* **1986**, *6*, 101.
(47) Bull, L. M.; Henson, N. J.; Cheetham, A. K.; Newsam, J. M.; Heyes, S. J. J. *Phys. Chem.* **1993**, *97*, 11776.
(48) Yashonath, S.; Santikary, P. *J. Phys. Chem.* **1994**, *98*, 6368.
(49) Kunze, K. L.; Davidson, E. R. *J. Phys. Chem.* **1992**, *96*, 2129.

charge estimates of metal hexacarbonyls are derived from quantum chemical population analysis[49] for $Mo(CO)_6$ [Mo, (+0.07); C, (+0.20); O, (−0.21)] and for $Cr(CO)_6$ [Cr (+0.15); C, (+0.18); O (−0.20)]. They are found to be in reasonable agreement with X-ray diffraction[50] and XPS experimental measurements.[51] We would like to point out that the polarizability interactions between $M(CO)_6$ and zeolite atoms have been neglected. This is expected to contribute not more than 15% to the total interaction. We believe that the results and in particular the trends reported here will remain unchanged on the inclusion of the polarizability interactions.

The Monte Carlo simulations at fixed loading (1 $M(CO)_6$ per unit cell) were carried out using the conventional Metropolis algorithm. This allows us to ignore $M(CO)_6$−$M(CO)_6$ interactions. One molecule is initially placed inside a micropore of the zeolite. One Monte Carlo step consists of a random displacement of the center of mass followed by an arbitrary rotation of the entire molecule. In order to eliminate the effect of boundaries we have used periodic boundary conditions with a period equal to one zeolite unit cell. A cutoff radius of 12 Å is applied to the Lennard-Jones interactions and the long-range electrostatic interactions are calculated using the Ewald summation technique.

The Monte Carlo simulations of the sorption and cosorption at fixed pressures were carried out using the grand canonical ensemble (GCMC), in which the number of particles in the system is determined by the fixed chemical potential of each species. One Monte Carlo step consists of four parts (create, destroy, translate, and rotate a molecule).

Results and Discussion

Sorption of $M(CO)_6$ in M'_nFAU Zeolites at Low Coverage. (a) DRIFTS Study. When the DRIFTS spectra were recorded immediately after the sorption of hexacarbonyl metal(0) $M(CO)_6$ (M = Cr, Mo, W) from the vapor phase into calcinated and vacuum thermally dehydrated M'_nFAU zeolites, all the spectra display a structureless broad band centered near 1980 cm^{-1},[10,22,52] and no splitting was observed upon cooling to 100 K. The DRIFTS spectra appear essentially invariant to the nature of the host. The particularity of the DRIFTS technique is its sensibility to the low coverage. Indeed, the coverages between 1 $M(CO)_6$ per 20 unit cells and 1 $M(CO)_6$ per 2 unit cells are detected without the saturation of the ν(CO) fundamentals. They can be assumed to be representative of the extreme dilution of $M(CO)_6$ within the zeolite. The fundamental ν(CO) patterns have a better resemblance to the ν(CO) spectra of the corresponding $M(CO)_6$ in solution, whereas no direct analogy was found with the bulk state of solid $M(CO)_6$.[53] The free octahedral $M(CO)_6$ molecule has three fundamental vibrations in the ν-(CO) region: nondegenerate $\nu_1(A_{1g})$ near 2120 cm^{-1} (Raman active); *doubly* degenerate $\nu_3(E_g)$ near 2020 cm^{-1} (Raman active), and *triply* degenerate $\nu_6(F_{1u})$ near 2000 cm^{-1} (infrared active). The IR activities, weak spectral shifts, and band broadenings indicate weak and isotropic interactions probably through adsorption on the outer surface of the microcrystals of zeolites and disorder of the guest in the porous void.

Upon standing, the original spectra progressively develop into more complex features typical of the zeolite host.[10,21,52] This can be explained in terms of a diffusion control of $M(CO)_6$ in the voids of the microcrystal to an order of the guests. The migration rate of $M(CO)_6$ within the pore system to a definite adsorption site is actually slow and can be increased under gentle warming.[10,21,52] For the purely siliceous FAU zeolite, at very low coverage when the system was allowed to reach equilibrium over 48 h at room temperature, only one ν(CO) absorption (1980 cm^{-1}) was observed, whereas at most six well-defined ν(CO) absorptions were detected for M'_nFAU, arising from the lifting of the different degeneracies. Significant narrowing of the bands was obtained upon cooling to 100 K (Figure 1). It is well-established on the basis of a number of chemical, NMR, and EXAFS investigations that sorption of $M(CO)_6$ into the M'_n-FAU zeolites (Si/Al > 2.5) at ambient temperature results in retention of the structural integrity of the $M(CO)_6$ over several months at room temperature.[10,21] It should be noted that the decomposition of $M(CO)_6$ into subcarbonyls occurred upon sorption into M'_nFAU zeolites (Si/Al < 2.5) even at room temperature.[8−10,24,54] Therefore, the sorption of $M(CO)_6$ in M'_n-FAU ($n \geq 85$) was carried out at 250 K and the spectra were run subsequently to avoid the intrazeolite decomposition of $M(CO)_6$. They exhibit a six-band ν(CO) pattern.

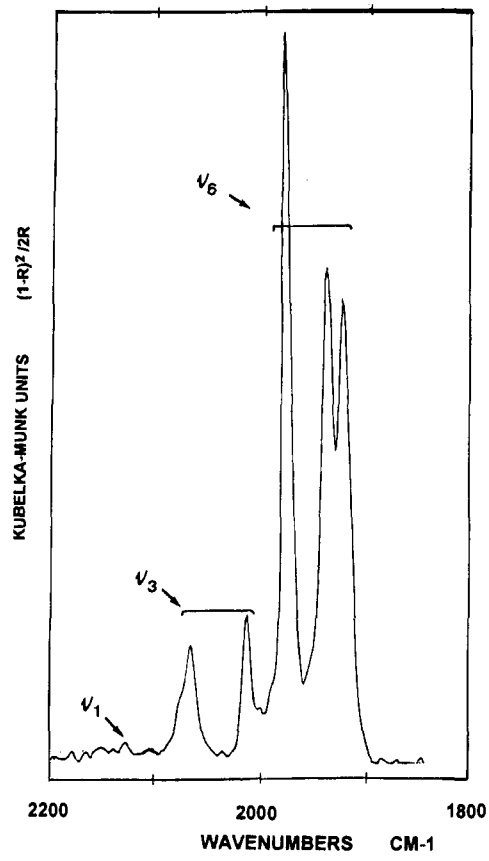

Figure 1. DRIFTS spectrum (100 K) in the fundamental ν(CO) region of $Mo(CO)_6$ occluded at low coverage in $Na_{56}FAU$ (1/20 unit cells).

At very low coverage, typically 1 $M(CO)_6$/20 unit cells of siliceous FAU, the sorption undergoes isotropic perturbation of the O_h symmetry which results in weak band broadening of the $\nu_6(F_{1u})$ infrared active mode. The similarity between the IR spectra of $M(CO)_6$ in solution and occluded in the siliceous FAU provides clear evidence that the motion of the $M(CO)_6$ molecule within the α-cage approaches at room temperature the rapid isotropic limit characteristic of a liquid.

In contrast, in zeolites M'_nFAU with $M' = Na^+$ and n in the 16−96 range, the DRIFTS spectra of the $M(CO)_6$ guest exhibits a six-well-defined ν(CO) absorption pattern which is characteristic of a well-defined adsorption site with a C_{2v} local symmetry, or lower.[10,21] The low local symmetry promotes the breakdown of the selection rules of the free molecule and induces the splitting of the $\nu_6(F_{1u})$ band into three components and the appearance of the $\nu_1(A_{1g})$ and the appearance and

(50) Bauschlicher, C. W., Jr.; Bagus, P. S. *J. Phys. Chem.* **1984**, *81*, 5889.
(51) Folkeson, B.; Larsson, R. *J. Electron. Spectrosc. Relat. Phenom.* **1990**, *81*, 5889.
(52) Zecchina, A.; Bordiga, S.; Platero, E. E.; Arean, C. O. *J. Catal.* **1990**, *125*, 568.
(53) Kariuki, D. A.; Kettle, S. F. A. *Inorg. Chem.* **1978**, *17*, 141 and references cited therein.
(54) Okamoto, Y.; Maezawa, A.; Kane, H.; Imanaka, T. *J. Chem. Soc., Faraday Trans. 1* **1989**, *84*, 851.

splitting of the $\nu_3(E_g)$ IR-forbidden modes of the free molecule, see Figure 1. Analogous spectroscopic behaviors were observed for zeolites ($16 < n < 96$) with the small cations $M' = Li^+$, Na^+, Mg^{2+}, and Ca^{2+}.

In the case of M'_nFAU ($n = 56$) with bulky cations such as $M' = K^+$, Rb^+, and Cs^+, the local symmetry of the guest was found to be C_{3v} with respect to the four observed $\nu(CO)$ absorptions. The two prominent bands arise from the splitting of the IR-active $\nu_6(F_{1u})$ mode into A_1 and E modes and the two weaker bands (A_1, E) arise from the IR-forbidden $\nu_1(A_{1g})$ and $\nu_3(E_g)$ modes of the free molecule, respectively.

(b) Monte Carlo Simulations. The spectroscopic results are supported by the Monte Carlo simulations of the sorption at "zero filling". In this case the sorbate−sorbate interactions do not take place. The energy of adsorption of $M(CO)_6$ in Na_n-FAU markedly depend on n. In the case of $Mo(CO)_6$, from $n = 0$ to 32 $\mathbf{U}_{ZS}$ decreases rapidly from −5 to −10 kcal mol^{-1}. In the $n = 32-64$ range, $\mathbf{U}_{ZS}$ is approximately constant (−12 kcal mol^{-1}), then from $n = 64$ to 96, $\mathbf{U}_{ZS}$ increases from −13 to −9 kcal mol^{-1}. These predictions reflect the dominating influence of the cation−sorbate interactions.

The positions occupied by $M(CO)_6$ in the completely siliceous FAU are mainly distributed between the four windows of the α-cages. The absence of a well-defined sorption site from the zero filling MC simulations of the sorption indicates that the net potential surface accessible to the molecule is fairly uniform, a finding that is consistent with the isotropic behavior observed from the DRIFTS experiments. $M(CO)_6$ is probably undergoing rapid rotational and translational motions upon the vibrational spectroscopy time scale.

In dehydrated dealuminated Na_nFAU ($n < 56$), the cation site preference is II > I′ > I, with site I almost completely empty.[34−36] Taking into account a statistical model of the distribution of cations on each site in the simulation box, the MC simulations of the sorption point out the location of $M(CO)_6$ near the 12-ring window site with a maximum number of surrounding cations ($n < 32$). This was confirmed by the simulation of the $Mo(CO)_6$ sorption in $Na_{56}FAU$ (32 Na^+ in site II and 24 Na^+ in site I′). Figure 2 depicts the most probable location of $Mo(CO)_6$ in $Na_{56}FAU$ at 273 K. More than 95% of the Mo center of mass sampled during the simulations is located within an isosurface of the probability density of Mo. This isosurface is approximately a 1.3 Å diameter sphere situated in the vicinity of the center of the window. These results show that there is a well-defined sorption site near the window of the supercage. $Mo(CO)_6$ located in such a window has a considerably lower energy than a molecule in the supercage. The occupancy of the cationic sites I and I′ was found to have a weak effect over the energy (∼1 kcal mol^{-1}) and was found to generate slight differences in the distribution of positions occupied by $Mo(CO)_6$. However, even after a large number of MC simulations, the residual MC step sizes remain large (translation 0.2 Å, rotation 8°), indicating some positional disorder in the vicinity of the window. The Mo atom is not located precisely, but it is distributed between the equivalent sites of the potential surface. The closest O(S)- - -O(Z) distances are found to be in the 4.3−2.4 ± 0.1 Å range and the six nearest Mo- - -Na^+ distances are found to be 5.9, 6.6, 6.6, 7.1, 7.1, and 7.7 ± 0.1 Å, respectively, the nearest O(S)- - -Na^+ distance being 2.7 ± 0.1 Å. The local symmetry was found to be close to C_{2v} and is in good agreement with the vibrational spectroscopic results (Figure 1). The locations of the sorbates were found analogous for all the $M(CO)_6$ molecules (M = Cr, Mo, W). It should be noted that the slight differences are probably

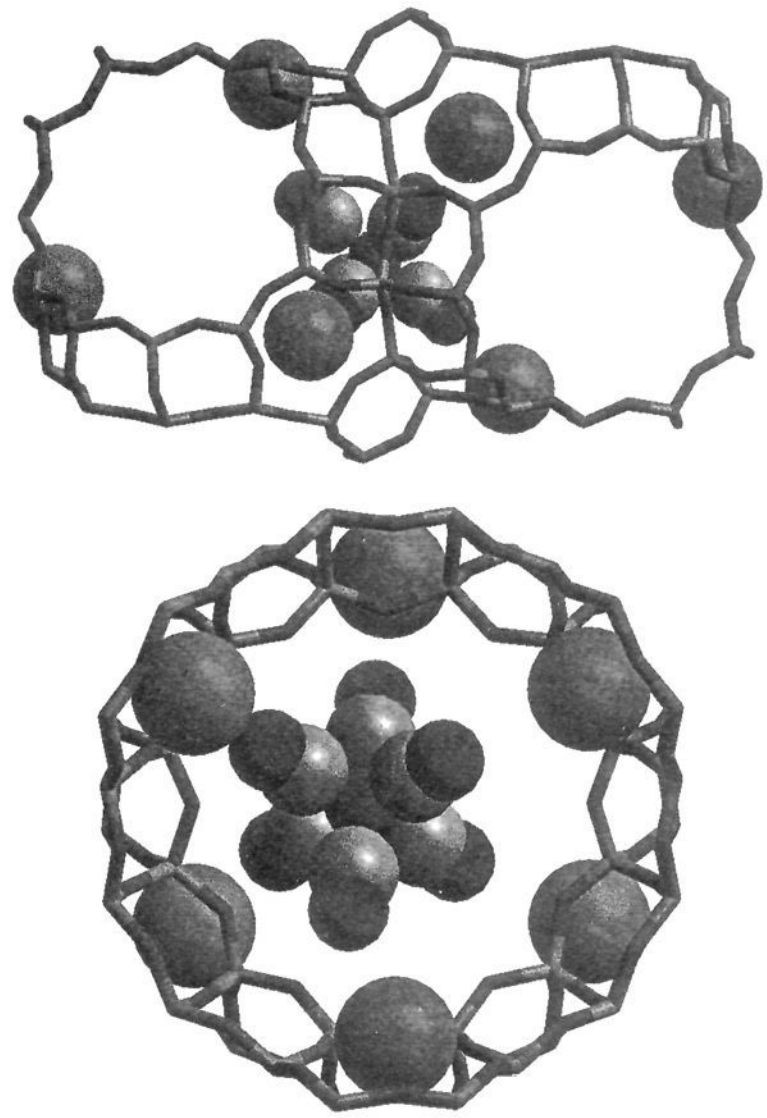

Figure 2. Predicted sorption site of $Mo(CO)_6$ in $Na_{56}FAU$ at "zero filling". (a, top) Two α-cages of zeolite $Na_{56}FAU$ and the interconnecting 12-ring window of diameter 8 Å. (b, bottom) In the plane of the 12-ring window. Black and shaded cylinders represent O and Si/Al atoms of the zeolite framework, respectively. The large shaded spheres represent Na^+, the medium black and shaded spheres represent O and C atoms of $Mo(CO)_6$, respectively.

generated by long-range electrostatic interactions through different sets of localized partial charges.[51]

The occupancy of the sites III by Na^+ cations in Na_nFAU with $n > 80$ promotes a significant destabilization of the $Mo(CO)_6$ location siting in the window through CO- - -Na^+ close contacts and consequently the stabilization of the location siting inside the supercage.

The substitution in $Na_{56}FAU$ of the Na^+ cations by cations such as Li^+, K^+, Rb^+, Cs^+, and Ca^{2+} modifies dramaticaly the sorption properties. With the set of potential values used the sorption energy of $Mo(CO)_6$ at "zero filling" varies markedly with the nature of M', particularly, −9.5 (Li^+), −16 (K^+), −20 (Rb^+), and −15 kcal mol^{-1} (Cs^+). The distribution of positions occupied by $Mo(CO)_6$ in $Li_{56}FAU$ is located deeper within the cage, but in the vicinity of the window with a degree of translational and rotational freedom (the residual MC step sizes are found to be 0.25 Å and 13° for translation and rotation, respectively). However, the low local symmetry was found to be in good agreement with the spectroscopic behavior at low coverage. The small size of Li^+ allows the location of $M(CO)_6$ deeper inside the cage. As the size of M′ increases from Li^+ to Cs^+, $M(CO)_6$ is constrained to reside in the center of the window with a C_{3v} local symmetry as deduced above from IR data. The isosurface of the probability density of the center of mass was reduced from a large region (2.2 Å size) in the vicinity of the window of $Li_{56}FAU$ to a spot (0.02 Å) in the center of the window of $Cs_{56}FAU$. However, it should be noted that the distribution of positions occupied by $M(CO)_6$ in M'_nFAU (M′ = Rb^+, Cs^+) deduced from MC simulations indicates a

supplementary broad sorption site near the center of the supercage with higher energy (−1 kcal mol^{-1}). The relevant experimental data concerning the structures of occluded carbonyl metals in zeolites are lacking. However, the interaction of intrazeolite $M(CO)_6$ with rubidium cations of the zeolite has been probed previously with rubidium edge EXAFS data.[10] The Fourier transformed data of the empty rubidium exchanged zeolite as well as those of the loaded sample appear to be very similar. These results suggest that the Rb^+ ions are mainly located in six ring positions of the zeolite. Moderate outershell scattering at ca. 4 Å observed in the Mo data could indicate the interaction between carbonyl ligands and site II Rb^+ ions. The geometrical parameters deduced from the simulation of the $Mo(CO)_6$ at "zero filling" in Rb_{56}FAU are in reasonable agreement with the EXAFS data.[10] The Mo atom is located on the crystallographic C_3 axis with each CO ligand directed toward each one of the six nearest Rb^+ cations. The predicted average Mo- - -Rb^+ distance was found to be 6.0 ± 0.1 Å whereas the average C(S)- - -Rb^+ and O(S)- - -Rb^+ distances were found to be 4.1 ± 0.1 and 2.9 ± 0.1 Å, respectively. The average distance between O(S)- - -O(Z) was found to be 2.9 ± 0.1 Å. In the case of Ca_{28}FAU, taking into account a statistical model of the distribution of cations on each site and occupancy factors deduced from X-ray data, the most probable location of $M(CO)_6$ was found to be inside the supercage with a maximum number of nearest Ca^{2+} cations. Two *trans* CO ligands are directed toward adjacent Ca^{2+} cations. The two nearest Mo- - -Ca^{2+} distances are found to be 5.2 ± 0.1 Å whereas the distances between Mo and the two remaining cations are 7.8 and 8.3 Å, respectively.

Sorption of $M(CO)_6$ in M'_nFAU Zeolite Hosts at High Coverage. (a) DRIFTS, ATR-FTIR, and Raman Scattering Studies. The experimental saturation loadings were found to be close to 16 $M(CO)_6$ (M = Cr, Mo, W) per unit cell for all the FAU zeolites. This finding is in good agreement with previous works.[8-10] Powder X-ray diffraction (XRD) studies of both the freshly loaded and equilibrated samples up to saturation filling display no evidence for bulk $M(CO)_6$ microcrystals. Neither does one observe any extra XRD lines or anomalous base line effects signaling any obvious degradation of the crystallinity of the zeolite, destruction of the framework, or formation of amorphous phases. Other spectral diagnostics of the guest and/or host were monitored by ATR-FTIR and Raman spectroscopies. The prominent vibrational characteristics of the aluminosilicate framework of the loaded and bare zeolites were found to be analogous, indicating no apparent modification of the structure and dynamic of the framework upon sorption. In addition, the ATR technique is particularly sensitive to the external surface of the zeolite particles.[32] Thus, after a brief evacuation of the loaded samples the broad band around 2000 cm^{-1} assigned to $M(CO)_6$ adsorbed onto the external surface of the particles was removed. Then, the ν(CO) patterns recorded using ATR-FTIR and crude sample or using DRIFTS and sample dispersed in dry NaA zeolite are identical and representative of the internal surface of the M'_nFAU zeolites.

The ν(CO) patterns of $M(CO)_6$ entrapped at high coverage in the purely siliceous FAU have a resemblance to the low-coverage spectra, except for some broadening probably introduced by the intermolecular CO−CO interactions. They exhibit a ν_6 broad band at room temperature; however, several ill shoulders have been detected at low temperature. As expected, the room temperature Raman spectra were found to be analogous to the corresponding spectra recorded using the concentrated solutions of $M(CO)_6$ as samples. We notice that the ν(CO) modes of the isolated $M(CO)_6$ yield $\nu_1(A_{1g})$ and $\nu_3(E_g)$ Raman-active bands, whereas the $\nu_2(A_{1g})$ and $\nu_{11}(F_{2g})$ Raman active modes are assigned respectively to M−C stretching and M−C−O deformation motions. All these prominent bands were clearly detected in the room temperature Raman spectra of $M(CO)_6$ occluded in FAU without any apparent modification. The partial splittings of the degenerate ν_6 and ν_{11} modes at low temperature indicate that the motions of $M(CO)_6$ within the cages slow down at low temperature and are in the range of the isotropic limit of a liquid only at room temperature.

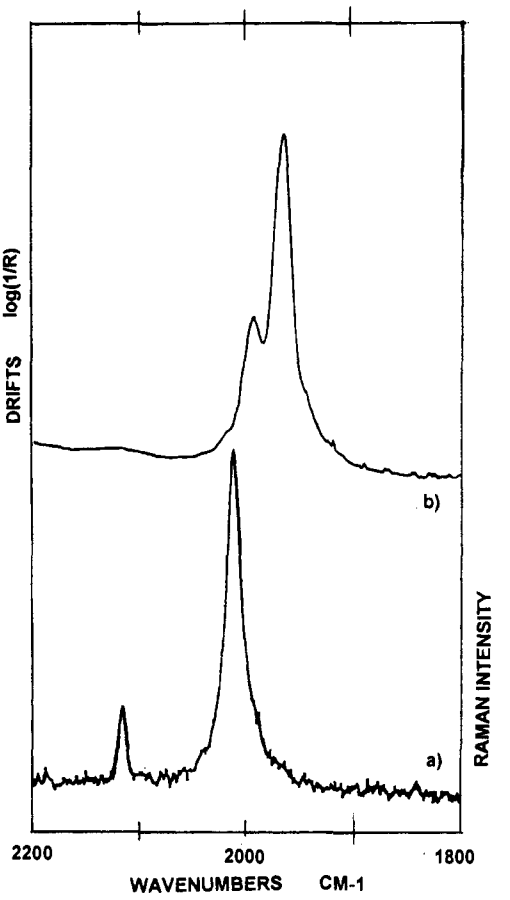

Figure 3. (a) Raman (300 K) and (b) DRIFT (300 K) spectra in the ν(CO) region (cm^{-1}) of $Mo(CO)_6$ occluded in K_{56}FAU at high coverage (16 $Mo(CO)_6$/unit cell).

In the case of aluminated zeolites M'_nFAU with large extraframework cations (M' = K^+, Rb^+, Cs^+) the DRIFTS spectra of occluded $M(CO)_6$ recorded at low and high coverage are analogous. The ν_6 band splits into two bands and the intracavity electrostatic field induced the IR-forbidden modes ν_1 and ν_3 as a weak band and a shoulder, respectively. These latter bands coincide with the prominent ν_1 and ν_3 Raman-active bands (Figure 3) whereas the weak shoulders in the ν(CO) Raman region coincide with the intense IR bands derived from the ν_6 mode. The low-frequency ν_2 and ν_{11} Raman active modes were observed in the expected regions, respectively. However, the splitting of the degenerate $\nu_{11}(F_{2g})$ mode is evident even at room temperature.

In the case of small cations such as M' = Li^+, Na^+, Mg^{2+}, and Ca^{2+}, the DRIFTS spectra of occluded $M(CO)_6$ exhibit more complex ν(CO) patterns at high coverage than at low coverage even after annealing and a long equilibration period (Figure 4). The supplementary splittings of the Raman and DRIFTS bands are more evident after spectral decomposition of the low-temperature spectra, Table 2. This aspect will be detailed in the following section. No such splittings were observed in the low-temperature Raman spectra in the ν_2 region of the ν(MC)

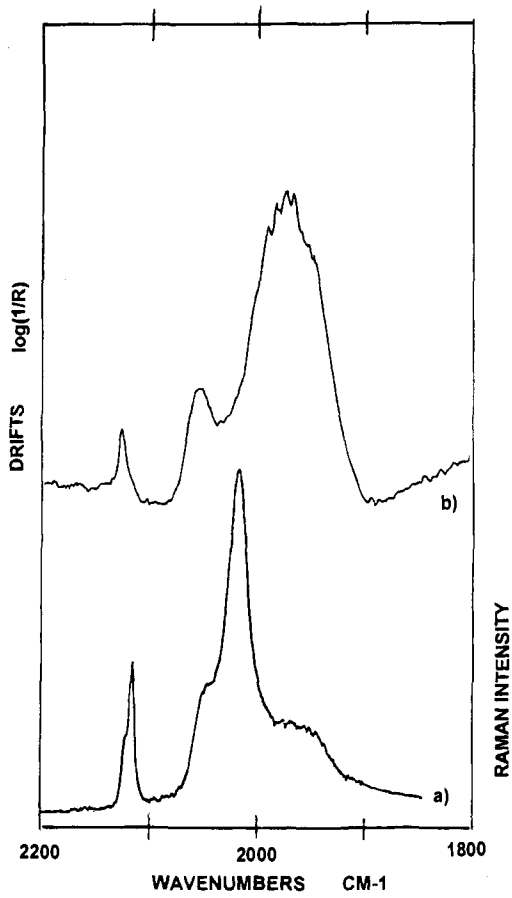

Figure 4. (a) Raman (300 K) and (b) DRIFT (300 K) spectra in the ν(CO) region (cm^{-1}) of $Mo(CO)_6$ occluded in $Na_{56}FAU$ at high coverage (16 $Mo(CO)_6$/unit cell).

Table 2. ν(CO) Frequencies (cm^{-1}) in the ν_1 and ν_3 Regions of $Mo(CO)_6$ Occluded at Saturation Filling in M'_nFAU Zeolites (M' = Li^+, Na^+ K^+, Rb^+, Cs^+, Mg^{2+}, Ca^{2+})

$\nu(CO)^a$	FAU	Li_{56}	Na_{56}	K_{56}	Rb_{56}	Cs_{56}	Mg_{28}	Ca_{28}
ν_1	2120	2123	2123				2124	2123
		2115	2116	2116	2116	2115	2116	2116
ν_3		2053	2053				2057	2054
		2034	2040				2045	2039
	2020	2023	2021				2030	2026
		2016	2014	2010	2013	2020	2018	2015

[a] Determined using spectral decomposition.

modes of $M(CO)_6$ occluded in M'_nFAU zeolites (M' = Li^+, Na^+) (Figure 5). Nevertheless, it should be noted that for M' = Mg^{2+} and Ca^{2+} the ν_2 Raman band broadens significantly and could be related to two different location sites. The Raman active modes assigned to the translational motions of the cations of the bare M'_nFAU have been detected previously below 120 cm^{-1} as weak bands by comparison with the most prominent band near 500 cm^{-1}.[29] These features were not detected in the Raman spectra of the corresponding loaded zeolites. With respect to the relative intensities, the additional weak Raman bands observed at 70 and 50 cm^{-1} for $Mo(CO)_6$ occluded in $Na_{56}FAU$ have been readily attributed to the external modes of the guests in their sites (Figure 5).[25] In contrast, the relatively intense far-IR cation modes are clearly detected in the spectra of the loaded zeolites at saturation filling. The spectral features of the cations are only weakly perturbed upon sorption of $M(CO)_6$. This finding, in good agreement with previous works,[10,13] reflects that the site symmetry and distribution of the cations remain practically unchanged upon sorption.

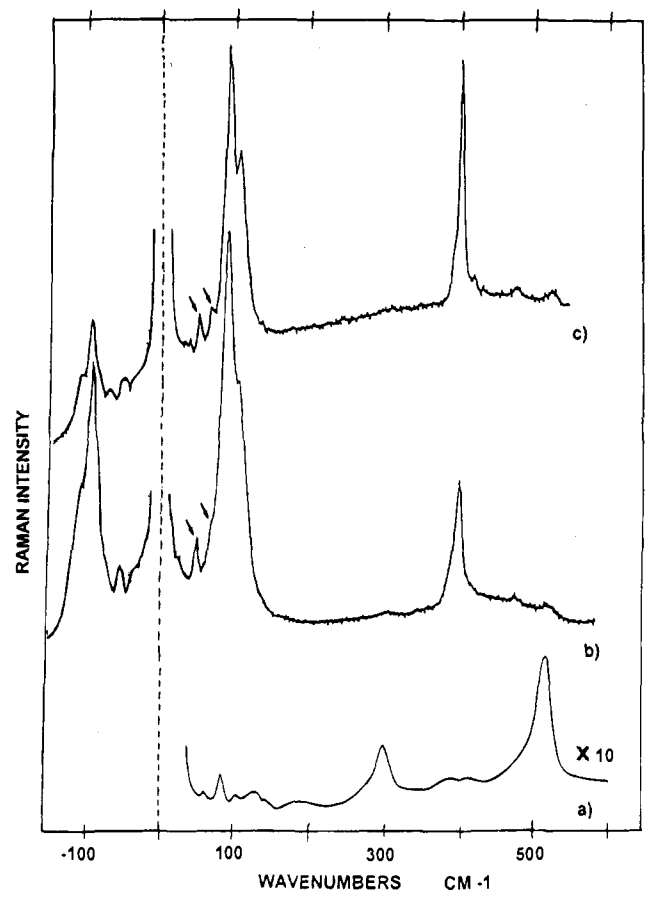

Figure 5. Low-frequency Raman spectra (cm^{-1}) in the Stokes and anti-Stokes regions of (a) bare $Na_{56}FAU$ (300 K), (b) $Mo(CO)_6$ (300 K) occluded in $Na_{56}FAU$ at high coverage (16 $Mo(CO)_6$/unit cell), and (c) $Mo(CO)_6$ (77 K) occluded in $Na_{56}FAU$ at high coverage (16 $Mo(CO)_6$/unit cell).

The DRIFTS study of the as-synthesized samples provided usable information about the IR-active overtones and combination of modes of occluded $M(CO)_6$. It appears that the anharmonicity of the vibrational modes of the entrapped $M(CO)_6$ remains weak upon sorption. The overtone DRIFTS spectra of the loaded M'_nFAU are typical of the hosts and some characteristic fundamental modes of the ν(MC) and δ(MCO) types were deduced from the spectroscopy of the overtones and combination modes.

(b) Grand Canonical Monte Carlo Simulations. The prediction of sorption at saturation filling was carried out at 300 K and 10 kPa constant pressure. For all the zeolites used, the calculated loadings corresponding to the filling of the voids were found to be 16 $M(CO)_6$ (M = Cr, Mo, W) per unit cell. These data are in good agreement the previous and present experimental values (elementary analyses, gravimetric methods, ^{129}Xe NMR measurements[55]). The energy of sorption (U_{ZS} + U_{SS}) at saturation filling of $Mo(CO)_6$ in Na_nFAU was examined as a function of n. (U_{ZS} + U_{SS}) decreases from −6 to −10 kcal mol^{-1} for n = 0 to 56 and then it decreases from −10 to −20 kcal mol^{-1} for n = 56 to 96. The average zeolite/sorbate energy at saturation filling provides evidence for the contribution of weak sorbate/sorbate interactions and significant cation/sorbate interactions.

In the completely siliceous FAU the distribution of the configurations generated in the GCMC simulations indicates the predominant occupancy of the windows of the supercage. However, the net potential surface accessible to the $M(CO)_6$

(55) Tway, C. L.; Apple, T. M. *Inorg. Chem.* **1992**, *31*, 2885.

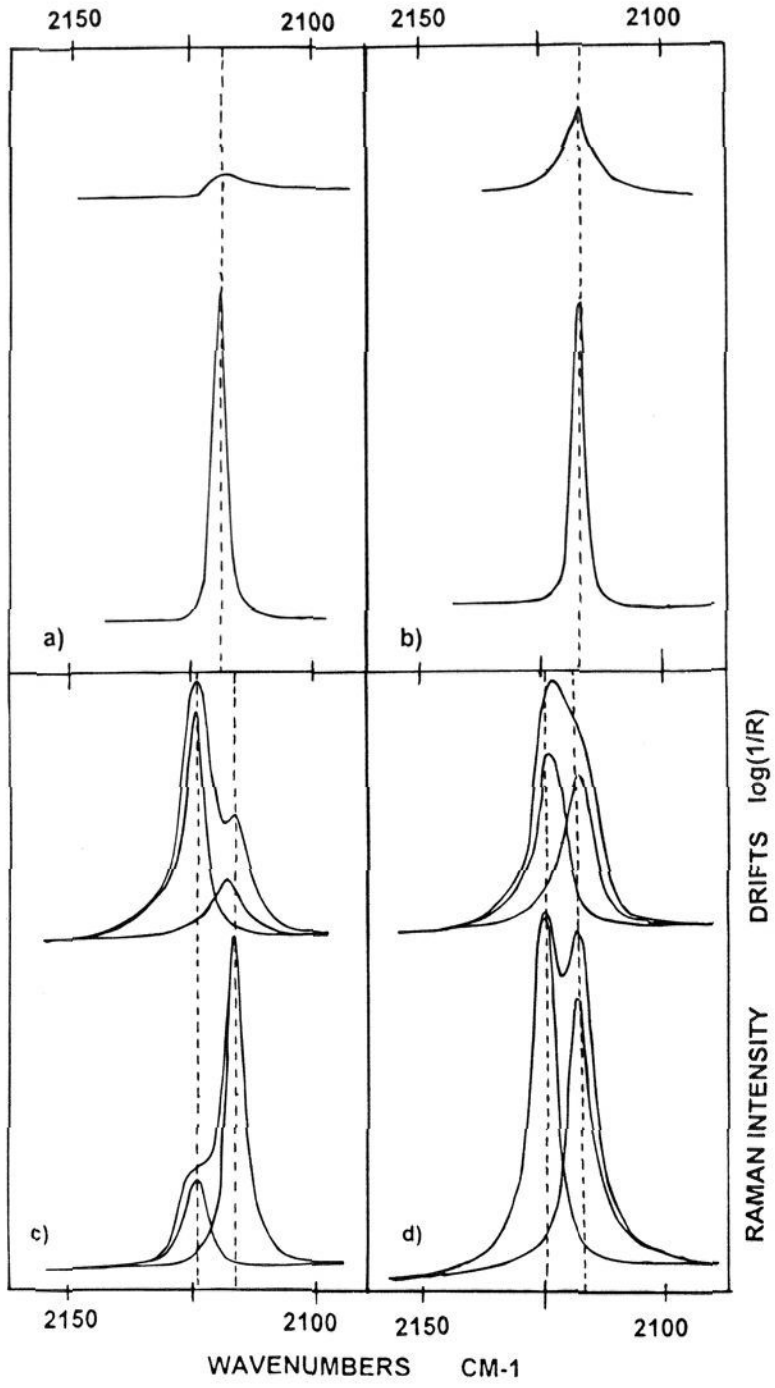

Figure 6. Raman (77 K) and DRIFT spectra (100 K) in the ν_1(CO) region (cm^{-1}) of $Mo(CO)_6$ occluded at high coverage (16 $Mo(CO)_6$/unit cell): (a) siliceous FAU, (b) K_{56}FAU, (c) Li_{56}FAU, and (d) Ca_{28}-FAU.

molecules is fairly uniform and $M(CO)_6$ experiences significant rotational and translational freedom in the porous void at room temperature as confirmed on the basis of the ν(CO) pattern.

At saturation loading, each $M(CO)_6$ is located in each 12-ring window of the supercages of M'_{56}FAU ($M' = Li^+$, Na^+, K^+, Rb^+, Cs^+, Ca^{2+}). Only one type of sorption site is found for each zeolite of the M'_{56}FAU type with alkaline cations. Thus, in the case of bulky cations (K^+, Rb^+, Cs^+) the predicted structural parameters found at "zero filling" remain unaffected at saturation loading (Figure 6) and all the closest Mo- - -Mo distances are found to be 8.7 ± 0.1 Å in K_{56}FAU host. In the case of smaller cations (Na^+, Li^+), the contoured regions of the distribution of positions of the center of mass M reduced only slightly from low coverage to saturation filling. They provide no clear evidence of the reduction of the translational and rotational freedom of the sorbates at saturation. However, the calculated structural parameters at complete filling (Figure 7) differ slightly from that predicted at "zero filling"; the three closest Mo- - -Mo distances were found to be in the range 6.7, 8.4, and 9.5 ± 0.1 Å, respectively, for the Li_{56}FAU host. In other words, the $M(CO)_6$ molecules associate in pairs in M'_{56}-FAU ($M' = Li^+$, Na^+), whereas in M'_{56}FAU ($M' = K^+$, Rb^+, Cs^+) the occluded $M(CO)_6$ can be considered as isolated molecule. In Ca_{28}FAU, the site II partial occupancy generates two types of sorption sites in the vicinity of the windows as deduced from the predicted interatomic distances and energy

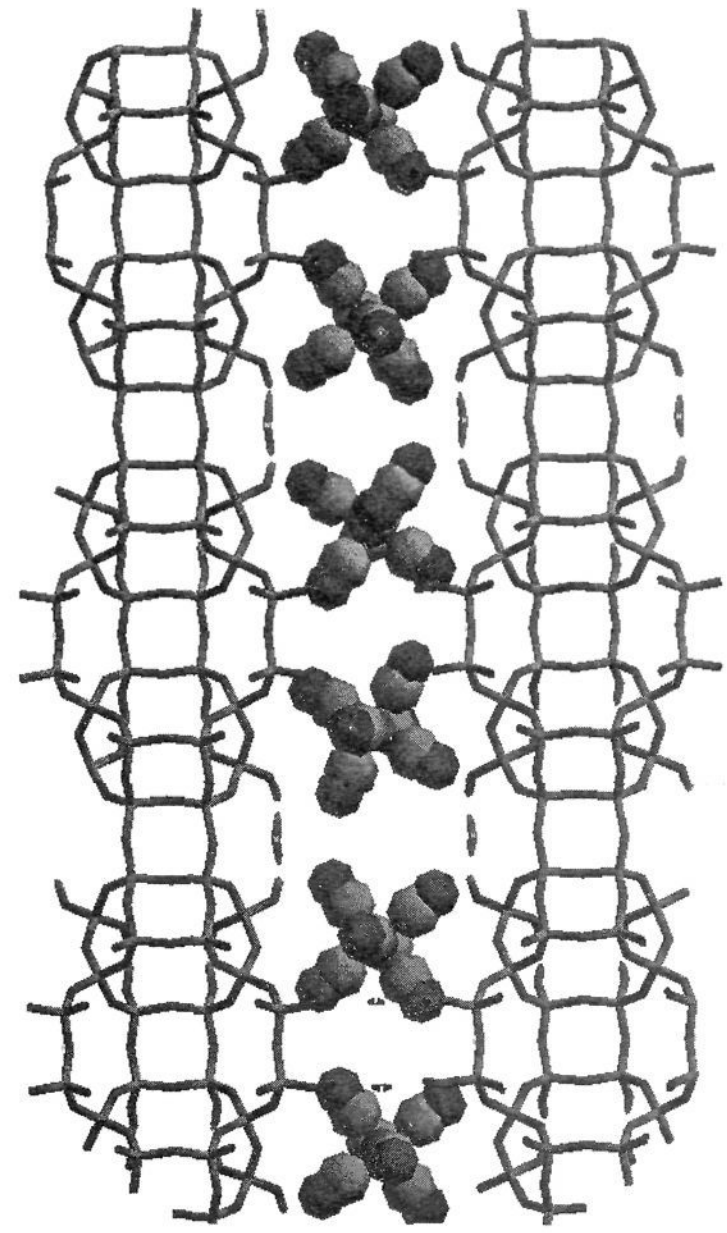

Figure 7. Z-clipping (thickness 10 Å) in the (010) plane showing the zeolite framework (black O and shaded Si,Al cylinders) and the predicted location of $Mo(CO)_6$ molecules along the channel, at saturation filling in K_{56}FAU (the extraframework K^+ cations are omitted for clarity).

distribution at saturation filling. The predicted sorption sites in the windows at saturation differ significantly from the predicted location within the supercage at zero filling. The prediction of the sorption of $M(CO)_6$ in Na_{96}FAU at high coverage remains purely speculative because of the intrazeolite decomposition. Nevertheless, it should be noticed that at high loading the sorbates are found to be located in the windows of the supercage in contrast to the location found to be inside the supercage at zero filling.

Cosorption of $M(CO)_6$ (M = Cr, W) into M'_nFAU Zeolite Hosts at High Coverage. Vibrational Coupling. Using natural-abundance compounds, it is possible that some of the splittings observed in the ν(CO) region of the IR spectra of $M(CO)_6$ occluded at high coverage in M'_nFAU ($M' = Li^+$, Na^+, Ca^{2+}, Mg^{2+}) are due to the presence of 6% of $M(^{12}C^{16}O)_5(^{13}C^{16}O)$ and 93% of $M(^{12}C^{16}O)_6$ species in the hexacarbonyl compounds. Some of the minor bands observed in the Raman and IR spectra of the compounds in the bulk state were readily assigned to ^{13}CO isotopic species. However, keeping in mind previous works concerning the ^{12}CO substitution[19] in $Mo(^{12}CO)_6$ entrapped in Na_{56}FAU by ^{13}CO and spectroscopic studies of isotopically ^{13}C-enriched $Mo(CO)_6$ crystals,[54] the supplementary splittings observed in both the Raman and IR ν(CO) patterns (Figure 6, Table 2) involve other major phenomena. In solution, the carbonyl stretching modes (ν(CO)) yield two Raman-active ($A_{1g} + E_g$) and one infrared-active (F_{1u}) bands. It is to be noted that the frequency corresponding to the totally symmetric A_{1g} mode is well separated from the E_g and F_{1u} frequencies. This

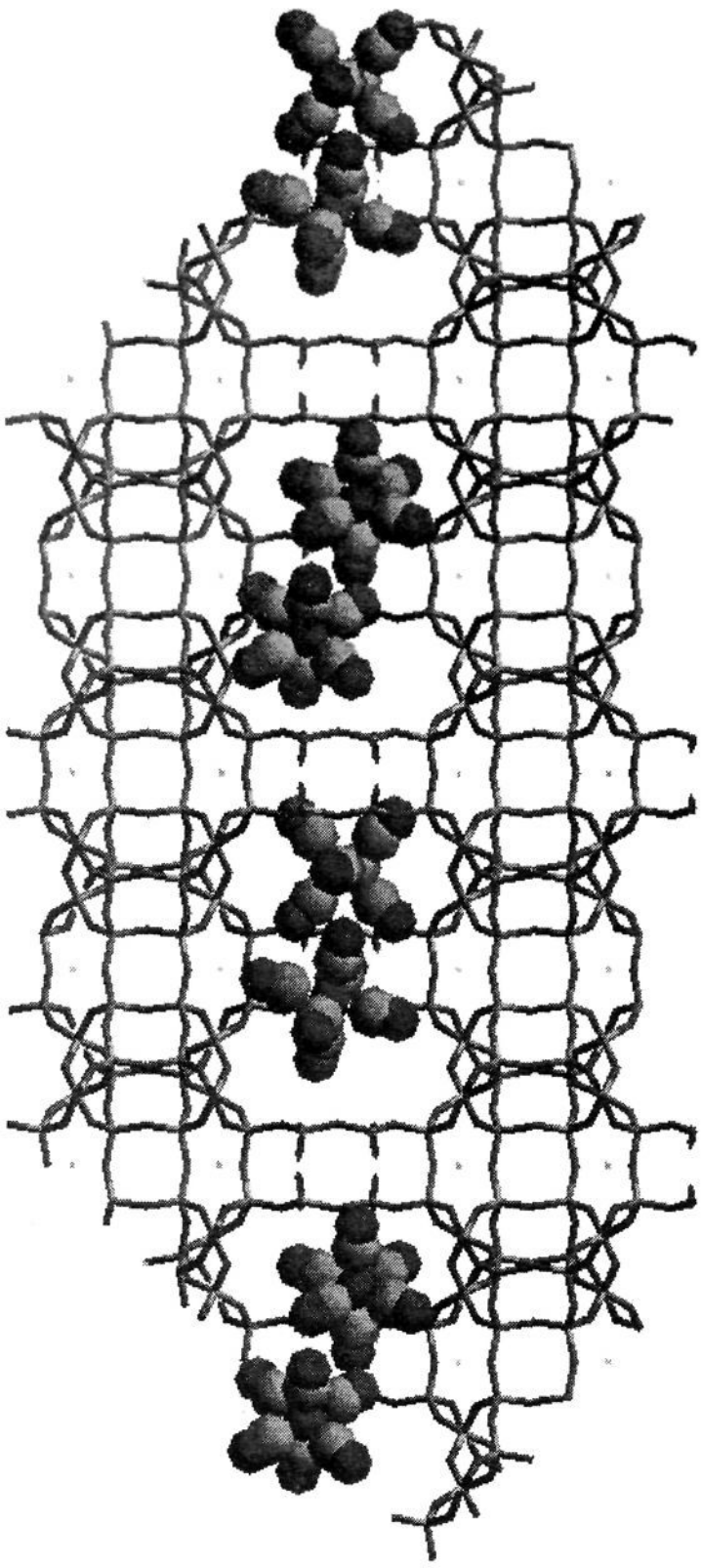

Figure 8. Z-clipping (thickness 10 Å) in the (010) plane showing the zeolite framework (black O and shaded Si,Al cylinders) and the predicted location of $Mo(CO)_6$ molecules along the channel, at saturation filling in $Li_{56}FAU$ (the extraframework Li^+ cations are omitted for clarity).

is because there is a strong interaction between the individual CO vibrators in an individual molecule. It is the existence of corresponding intermolecular interactions which give rises to the additional splittings in the vibrational spectra of the samples loaded at high coverage. The only evident alternative is that of the existence of two slightly different sorption sites in the void space of the zeolite. It is recognized that not all ν(CO) vibrations of metal carbonyl species couple in the crystalline state, although the rules determining whether a particular mode couples or does not are not completely clear.[54] As a general rule, those modes with strong transition dipoles (and so associated with an intense infrared absorption) would be expected to show the greatest coupling in the solid state.

In order to demonstrate the existence or the nonexistence of the intermolecular coupling through the ν(CO) modes the cosorption of $Cr(CO)_6$ and $W(CO)_6$ was undertaken into Na_{56}-FAU and $Rb_{56}FAU$ zeolites. The series $Cr_xW_{1-x}(CO)_6$ was studied in more detail than the others because the ν(CO) frequency separation, approximately 6 cm^{-1} (Table 3), of sorbed

Table 3. ν(CO) Frequencies (cm^{-1}) in the ν_1, ν_3, and ν_2 Regions of Sorbed $M(CO)_6$ (M = Cr, Mo, W) and Cosorbed $Cr(CO)_6$, $W(CO)_6$ (50%, 50%) at Saturation Filling in $Na_{56}FAU$ Zeolite

$M(CO)_6$	ν_1[a]		ν_3[a]				ν_2
sorption							
Cr	2118	2113	2056	2042	2030	2020	377
Mo	2123	2116	2053	2040	2021	2014	399
W	2125	2118	2044	2030	2018	2012	424
cosorption							
$Cr_{0.5}W_{0.5}$	2122	2116	2048	2040	2020	2014	377 424

[a] Determined using spectral decomposition.

(Cr) from sorbed (W) is larger than that for (Mo)−(Cr) and (W)−(Mo) compounds, respectively. The Raman spectra of both the mechanical mixtures and the cosorbed samples were carefully recorded at low temperature. The Raman spectra of the mechanical mixtures of $Cr(CO)_6$ and $W(CO)_6$ sorbed separately are the superposition of the pure components, where the band intensities only change with the concentration of each member. The spectra of $Cr(CO)_6$−$W(CO)_6$ cosorbed in Na_{56}-FAU are not the superposition of the pure components, in the ν(CO) region, Table 3. The number of ν(CO) bands of the $Cr_{0.5}W_{0.5}(CO)_6$−$Na_{56}FAU$ sample is identical to the number of ν(CO) bands of the $Cr(CO)_6$−$Na_{56}FAU$ or $W(CO)_6$−$Na_{56}FAU$ sample. In addition the band frequencies of the cosorbed sample were found to be intermediate between the frequencies of one member to that of the other one, respectively, the relative intensity remaining pratically identical. It is clear that in the (molecular) A_{1g}, E_g, and F_{1u} ν(CO)-derived region the intermolecular vibrational coupling is of sufficient magnitude to give a spectrum for which the peak frequencies are intermediate between those of the pure components. In contrast, the spectra of $Cr(CO)_6$−$W(CO)_6$ cosorbed into $Rb_{56}FAU$ and the corresponding mechanical mixtures are identical and are the superposition of the pure components. In the low-frequency region the spectral features of the cosorbed species in M'_nFAU ($M' = Na^+$, Rb^+) are, essentially, the superpositions of the spectral features of the pure components (Table 3).

The GCMC simulations of the $Cr(CO)_6$−$Mo(CO)_6$ cosorption were carried out at 300 K and 3 kPa in $Na_{56}FAU$ and Rb_{56}-FAU. At saturation filling, 8 $Cr(CO)_6$ and 8 $Mo(CO)_6$ molecules were found to be located in the unit cell of $Na_{56}FAU$ as Cr-$(CO)_6$−$Mo(CO)_6$ pairs rather than as $M(CO)_6$−$M(CO)_6$ (M=Cr or Mo) pairs, whereas the 8 $Cr(CO)_6$ and 8 $Mo(CO)_6$ molecules are randomly distributed in all the centers of the supercages of $Rb_{56}FAU$. Now, we think that it is physically realistic to postulate the occurrence of one type of sorption site within the M'_nFAU zeolites ($M' = Li^+$, Na^+) which gives rise to identical vibrational frequencies. Both supplementary frequency splittings and intensity changes occur in the IR and Raman ν(CO) patterns ($M' = Li^+$, Na^+) as a result of intermolecular couplings through ν(CO) modes between two $M(CO)_6$ in close proximity. The comparison between the corresponding Raman scattering and DRIFTS intensities of ν(CO) bands, particularly in the ν_1 region (Figure 8), indicates a nearly centrosymmetric structure of the $M(CO)_6$−$M(CO)_6$ pairs in Li_{56} and $Na_{56}FAU$ zeolites as predicted by GCMC calculations. In addition, one can deduce from the insensibility of the vibrational spectra to the loading of aluminated M'_nFAU ($M' = K^+$, Rb^+, Cs^+) that the vibrational coupling effects between guests in different windows are minimal. Two types of sorption sites were found within the M'_nFAU zeolites ($M' = Mg^{2+}$, Ca^{2+}) which give rise to different vibrational frequencies (Table 2). The band splittings are observed clearly in the Raman ν(CO) pattern. However,

intensity transfers probably occur through vibrational couplings between species in close proximity.

Earlier, it was demonstrated using mixed crystals derived from $M(CO)_6$ (M = Cr, Mo, W) and for $Mo(^{13}CO)_x(^{12}CO)_{6-x}$ that in the bulk state the intermolecular vibrational coupling occurs through the ν(CO) E_g-derived modes; no significant coupling through the A_{1g}-derived modes was detected. In the bulk state each $M(CO)_6$ molecule retains a symmetry close to O_h symmetry then the lowest multiple term connecting two A_{1g} modes is hexadecapole−hexadecapole whereas the lowest term connecting two E_g modes is quadrupole−quadrupole. In contrast, the intrazeolite electrostatic field induces a dipolar moment in the occluded $M(CO)_6$ molecules. The intermolecular vibrational coupling through the ν(CO) modes observed in the Raman and DRIFT spectra of $M(CO)_6$ occluded at high coverage in M'_n-FAU (M' = Li^+, Na^+) can be attributed to dipole−dipole interactions.

The spectroscopic results and MC simulations reveal that the $M(CO)_6$ molecules are not held rigidly in place in purely siliceous FAU even at high loading but are instead undergoing some form of rapid motion within the zeolite cages and windows. The rapid motions average the vibrational couplings as found in solution and broaden the IR and somewhat the Raman bands. $M(CO)_6$ does exhibit reduced mobility in aluminated M'_nFAU; the mobility depends mainly on the vacant space available for the guests in the intracrystalline voids. In M'_{56}FAU (M' = Li^+, Na^+) the intracrystalline voids permit $M(CO)_6$ associated in pairs. On the basis of ^{95}Mo T_1 measurements on samples of $Mo(CO)_6$ encapsulated in dried Na_{56}FAU, it was confirmed earlier that $Mo(CO)_6$ experiences significant rotational freedom in the zeolite supercages and the ambient temperature rotational correlation time, τ_c, is approximately 3 orders of magnitude longer than τ_c in solution.[20]

$M(CO)_6$ Loading-Dependent Effects in M'_nFAU and Distribution of the Guest Molecules in the Intrazeolite Voids. The average filling of the accessible α-cages of M'_nFAU following exposure times to $M(CO)_6$ was obtained by elementary analyses and probed by DRIFTS at low coverage and DRIFTS, ATR-FTIR, and Raman scattering at higher coverage. The experiments were conducted from 1 $M(CO)_6$/20 unit cells to saturation (16 $M(CO)_6$/unit cell). An important recurring question that arises in the study of occluded sorbates is one regarding the location and number of guest molecules trapped in the voids of the host. Multiple-quantum NMR specroscopy is known to be effective in determining the spacial distribution of hexamethylbenzene and other protonated molecules sorbed in zeolites.[56,57] The vibrational spectroscopy can also be used to probe the local molecular environment; on the other hand, the molecular simulations using GCMC calculations at low fixed pressures provide a significant picture of the molecular distribution in the cavities.

Following such a vapor phase transfer procedure, a prolonged thermal annealing, and evacuation one finds that the ν(CO) patterns remain essentially invariant to the $M(CO)_6$ coverage in purely siliceous FAU—the broadening of the ν(CO) bands as a function of the filling is in good agreement with interactions between molecules undergoing rapid motions within the voids. This finding is consistent with the inability to locate any sorbate in FAU by MC simulations.

In M'_{56}FAU with bulky cations (M' = K^+, Rb^+, Cs^+), the vibrational spectra are essentially invariant to the $M(CO)_6$ coverage. The vibrational spectroscopic behavior reveals that $M(CO)_6$ are rigidly held within the window of the supercage and vibrate independently from each other. The GCMC simulations at low fixed pressure indicate that the sorption sites in the center of the windows of the supercages are randomly filled as much as at saturation without any significant sorbate−sorbate interactions.

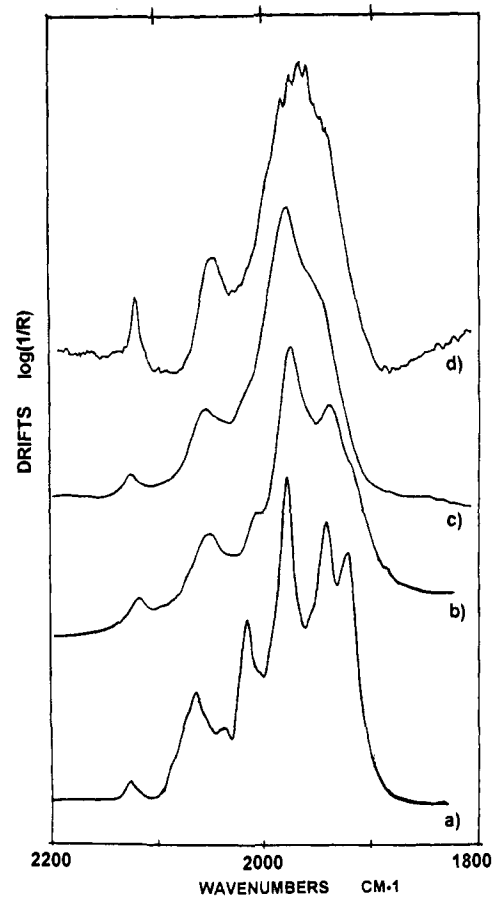

Figure 9. DRIFT spectra (300 K) in the fundamental ν(CO) region of $Mo(CO)_6$ occluded in Na_{56}FAU: (a) 1 $Mo(CO)_6$/20 unit cells, (b) $Mo(CO)_6$/8 unit cells, (c) 3$Mo(CO)_6$/1 unit cell, (d) 16 $Mo(CO)_6$/1 unit cell (dispersed in dry NaA zeolite).

In contrast, for aluminated zeolites with small cations (M' = Li^+, Na^+, Mg^{2+}, Ca^{2+}) the DRIFTS ν(CO) patterns change markedly as the average loading is increased from 1 $M(CO)_6$/20 unit cells to 4 $M(CO)_6$/unit cell, namely M = Mo in Figure 9, whereas the DRIFTS, ATR-FTIR, and Raman spectra change hardly at all as the loading is increased from 4 $M(CO)_6$/unit cell to saturation (16 $M(CO)_6$/unit cell). The ν(CO) wavenumber values of $Mo(CO)_6$ occluded in Na_{56}FAU change from 2126 (ν_1) and 2060, 2015 cm^{-1} (ν_3) at low coverage to 2123, 2115 (ν_1) and 2053, 2035, 2021, 2014 cm^{-1} (ν_3) at saturation filling, respectively. From DRIFTS results (Figure 9) and GCMC simulations at low fixed pressure, it is suggested that $Mo(CO)_6$ molecules are predominently entrapped as isolated molecules in Na'_{56}FAU at bulk concentrations lower than 4 $Mo(CO)_6$/unit cell, whereas at higher bulk concentrations the intracavity distribution is primarily pairwise. With an average number of density of 8 $Mo(CO)_6$ molecules per unit cell the vibrational spectroscopy and the GCMC simulations reveal that in the simulation box (1 unit cell), 5 supercages can be considered to be occupied by 1 $M(CO)_6$, 2 supercages are occupied by a $M(CO)_6$ pair, and 1 supercage is unoccupied. The intra- and intercavity mobility of the guest molecules within the intracrystalline voids depends on the available vacant space. How-

(56) Chemla, B. F.; Pearson, J. G.; Liu, S. B.; Ryoo, R.; de Menorval, L. C.; Pines, A. *J. Phys. Chem.* **1991**, *95*, 303.
(57) Hong, S. B.; Cho, H. M.; Davies, M. E. *J. Phys. Chem.* **1993**, *97*, 1622.

ever, the dynamic aspect of the study falls beyond the scope of the present work, but is in progress.

Conclusions

Molecular simulations of the sorption and cosorption energetics and siting locations of hexacarbonyl metals(0) $M(CO)_6$ (M = Cr, Mo, W) in faujasitic M'_nFAU zeolites (M' = Li^+, Na^+, K^+, Rb^+, Cs^+, Ca^{2+}, Mg^{2+}; $n = 0-96$) have been presented in combination with the DRIFTS, ATR-FTIR, and Raman scattering experimental study.

From the grand canonical ensemble Monte Carlo techniques (GCMC) reported here and experimental results reported here and in the literature a coherent picture of the sorption and cosorption of $M(CO)_6$ in M'_nFAU zeolites can be drawn, including a molecular level explanation of the steps of the sorption as a function of the Si/Al ratio of the zeolite framework, size and number of the extraframework cations M', and the coverage.

The positions occupied by $M(CO)_6$ in the completely siliceous FAU zeolite ($n = 0$) are randomly distributed in the windows of the α-cages. From low coverage to the saturation filling, the $M(CO)_6$ molecules are undergoing rapid translational and rotational motions at room temperature upon the time scale of the vibrational spectroscopy.

In aluminated zeolites ($n > 0$), the average zeolite/sorbate energy calculations provide evidence to the contribution of significant site II cation/sorbate interactions whereas site I,I' cation/sorbate and sorbate/sorbate interactions remain weak.

In $M'_{56}FAU$ zeolites with bulky cations (M' = K^+, Rb^+, Cs^+) the $M(CO)_6$ molecules are rigidly held to the six octahedrally disposed site II cations within the windows of the supercages and vibrate independently from each other. The sorption sites are randomly filled from low coverage to saturation.

In $M'_{56}FAU$ zeolites with small cations (M' = Li^+, Na^+) the distribution of positions occupied by $M(CO)_6$ is located in the vicinity of the windows. It is suggested that $M(CO)_6$ is predominently entrapped as an isolated molecule at low coverage whereas at higher bulk concentration the intracavity distribution is primarily pairwise.

In $M'_{28}FAU$ zeolites with site II partial occupancy (M' = Mg^{2+}, Ca^{2+}) the distribution of positions occupied by $M(CO)_6$ is located in the vicinity of the windows in two different sorption sites.

JA944188W